· Article · Advances in Polar Science
doi: 10.13679/j.advps.2021.0017 March 2022 Vol. 33 No. 1: 14-27

Effects of sea ice melt water input on phytoplankton biomass and community structure in the eastern Amundsen Sea

FENG Yubin, LI Dong*, ZHAO Jun, PAN Jianming, ZHANG Haisheng, HAN Zhengbing & ZHU Qiuhong

Second Institute of Oceanography, Ministry of Natural Resources (MNR), Hangzhou 310000, China

Received 6 May 2021; accepted 28 July 2021; published online 30 September 2021

Abstract Sea ice melt water and circumpolar deep water (CDW) intrusion have important impacts on the ecosystem of the Amundsen Sea. In this study, samples of nutrients and phytoplankton pigments from nine stations in the eastern Amundsen Sea were collected during the austral summer. Based on in-situ hydrological observations, sea ice density data from satellite remote sensing, and chemical taxonomy calculations, the relationships between environmental factors and phytoplankton biomass and community structure were studied. The results showed that with increasing latitude, the contribution of sea ice melt water (MW%) and the stability of the water body increased, and the depth of the mixed layer (MLD) decreased. The integrated concentration of chlorophyll *a* (Chl-*a*) ranged from 21.4 mg·m^{-2} to 148.4 mg·m^{-2} (the average value was 35.7±53.4 mg·m^{-2}). Diatoms (diatoms-A [*Fragilariopsis* spp., *Chaetoceros* spp., and *Proboscia* spp.] and diatoms-B [*Pseudonitzschia* spp.]) and *Phaeocystis antarctica* were the two most widely distributed phytoplankton groups and contributed 32%±16% and 28%±11%, respectively, of the total biomass. The contributions of Dinoflagellates, Chlorophytes, Cryptophytes, the high-iron group of *P. antarctica*, and Diatom group A were approximately 17%±8%, 15%±13%, 9%±6%, 5%±9%, and 3%±7%, respectively. The area with the highest phytoplankton biomass was located near the ice-edge region, with a short time lag (T_{lag}) between sampling and complete sea ice melt and a high MW%, while the area with the second-highest Chl-*a* concentration was located in the area affected by the upwelling of CDW, with thorough water mixing. Vertically, in the area with a short T_{lag} and a shallow MLD, the phytoplankton biomass and proportion of diatoms decreased rapidly with increasing water depth. In contrast, in the region with a long T_{lag} and limited CDW upwelling, the phytoplankton community was dominated by a relatively constant and high proportion of micro phytoplankton, and the phytoplankton biomass was low and relatively stable vertically. Generally, the phytoplankton community structure and biomass in the study area showed high spatial variation and were sensitive to environmental changes.

Keywords **Amundsen Sea**, **sea ice melt water**, **mixed layer depth**, **phytoplankton**, **pigments**, **biomass**

Citation: Feng Y B, Li D, Zhao J, et al. Effects of sea ice melt water input on phytoplankton biomass and community structure in the eastern Amundsen Sea. Adv Polar Sci, 2022, 33(1): 14-27, doi: 10.13679/j.advps.2021.0017

1 Introduction

The Southern Ocean is a key region for the absorption of atmospheric carbon dioxide and plays an important role in global circulation and carbon cycling (Sabine et al., 2004; Landschützer et al., 2016). The marginal ice zone surrounding the Antarctic continent is the most productive region in the Southern Ocean, with abundant phytoplankton primary production (Petrou et al., 2016) and a simple food chain (algae, krill, and top predators) (Ainley et al., 2005)

* Corresponding author, ORCID: 0000-0002-5470-4594, E-mail: lidong@sio.org.cn

due to its hydrological and nutrient conditions (Cheah et al., 2017). In the Antarctic continental marginal seas, diatoms and *Phaeocystis antarctica* have been proven to be the two most widely distributed algae and are considered to be the matter and energy base of the marine ecosystem (Schofield et al., 2017). Based on the dense silica shells and fast settling speed of diatoms (Sarthou et al., 2005) as well as the efficient dissolved carbonate absorption capacity of *P. antarctica* (Rost and Riebesell, 2004), these two types of phytoplankton contribute greatly to the vertical delivery of atmospheric carbon dioxide through the biological carbon pump. Under these circumstances, it is very important to explore the dynamics of these two important phytoplankton groups and their responses to the changing marine environmental conditions.

The Amundsen Sea is one of the most productive Antarctic continental marginal seas (Arrigo and van Dijken, 2003), is undergoing rapid environmental changes (including decreases in glacier size, attenuation of the ice shelf, and rapid sea ice retreat) (Cavalieri and Parkinson, 2008; Tortell et al., 2012), and has become the region with the fastest sea ice retreat rates in the Southern Ocean (Pritchard et al., 2012; Konrad et al., 2018). In the Amundsen Sea, the stronger intrusion of modified circumpolar deep water (CDW) will accelerate the melting of the ice shelf bottom (Rignot et al., 2013). Additionally, the decreasing sea ice area and shortening sea ice duration under the context of global warming will strongly affect the formation and dispersal of ice melt water, which play an important role in regulating the hydrodynamic conditions (such as water stratification) and trophic status of seawater (including the dissolved Fe supply) (Alderkamp et al., 2012; Fragoso and Smith, 2012; Rignot et al., 2013; Feng et al., 2021). Despite different degrees of affinity to the sea ice, the changes in the regional climate and sea ice dynamics could affect the biological activities of organisms at all trophic levels (from primary producers and zooplanktonic organisms to fish) (Ducklow et al., 2012). However, the studies on the distribution of phytoplankton biomass, community, and physiological characteristics have mainly been conducted in the shallow continental shelf region of the western Amundsen Sea (Alderkamp et al., 2012; Lee et al., 2016), and there are large gaps in our understanding of the spatial phytoplankton dynamics in terms of abundance and structure in the eastern Amundsen Sea. Compared to the continental shelf region of the western Amundsen Sea, the eastern Amundsen Sea is more adjacent to the Bellingshausen Sea, which is suffering the marked intrusion of CDW (Schmidtko et al., 2014). The eastern Amundsen Sea is therefore an ideal place to study the response of the phytoplankton community to the changing environmental conditions.

In order to study the spatial dynamics of phytoplankton stocks, phytoplankton pigment samples were collected from the water column in the eastern Amundsen Sea. The hydrological data (potential temperature and salinity), macro-nutrients (nitrate, phosphate, and silicate), and remote sensing data (sea ice density data) were obtained to study the spatial characteristics of environmental factors. The chemical taxonomy (CHEMTAX) method was performed to statistically evaluate the phytoplankton structure. This study aimed to explore the spatial dynamics of phytoplankton stocks and structure and their response to variations in environmental conditions, especially to the sea ice melt water input in this fast-warming region.

2 Material and methods

2.1 Field sampling and oceanographic measurements

Water and phytoplankton pigment samples were collected at nine stations in the eastern Amundsen Sea during the austral summer from January 13 to January 21, 2019 (Figure 1 and Table 1) as a part of the 35th Chinese National Antarctic

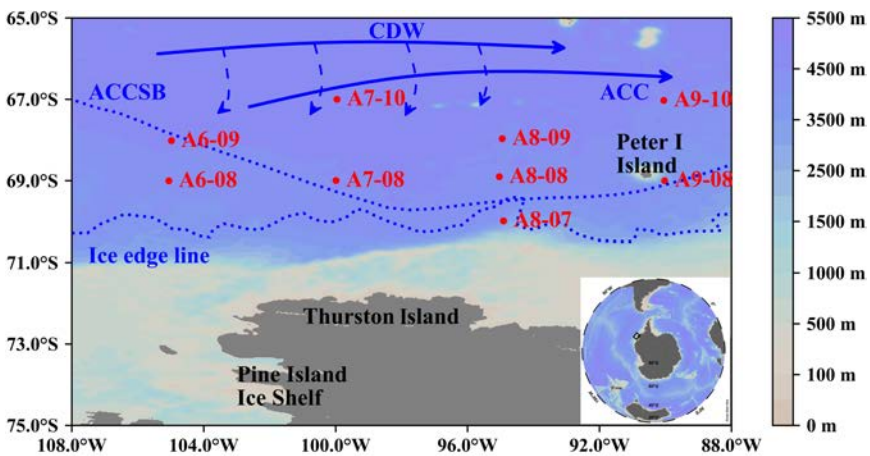

Figure 1 Study stations, ocean currents, and sampling locations. CDW: Circumpolar Deep Water; ACC: Antarctic Circumpolar Current; ACCSB: The Southern Boundary of the Antarctic Circumpolar Current (Tynan, 1998). Ice edge line: the area south of the ice-edge line was covered by sea ice. Blue solid line: the ocean current. Blue dashed line: the intrusion of CDW.

Table 1 Sampling station information

Station	Longitude	Latitude	Sampling date (DD-MM-YYYY)	Date of sea ice melt (DD-MM-YYYY)	Time lag/d
A6-08	105.06°W	68.99°S	13-01-2019	22-12-2018	22
A6-09	104.98°W	68.01°S	13-01-2019	07-12-2018	37
A7-08	99.99°W	68.99°S	15-01-2019	22-12-2018	24
A7-10	99.96°W	66.99°S	14-01-2019	01-11-2018	74
A8-07	94.91°W	69.99°S	21-01-2019	21-01-2019	0
A8-08	95.04°W	68.90°S	16-01-2019	27-12-2018	20
A8-09	94.95°W	67.97°S	16-01-2019	03-11-2018	74
A9-08	90.03°W	68.99°S	18-01-2019	14-01-2019	4
A9-10	90.05°W	67.03°S	17-01-2019	01-11-2018	77

Note: Time lag = Time between sampling and sea ice melting.

Research Expedition onboard R/V *Xuelong*. Water samples were collected with Niskin bottles attached to a rosette sampler at the surface and at depths of 25, 50, 100, and 200 m. The hydrological parameters (potential temperature, salinity, and potential density) were recorded by a Sea-Bird SBE-9/11 plus CTD (conductivity–temperature–depth) system (Bellevue, WA, USA), which was pre-calibrated (Figures 2 and 3).

2.2 Nutrient analysis

Seawater samples were filtered through acid-cleaned and pre-washed cellulose acetate membranes (0.45 μm) to determine dissolved inorganic nutrients (nitrate (NO_3^-), nitrite (NO_2^-), ammonium (NH_4^+), phosphate (PO_4^{3-}), and silicate (Si $(OH)_4$)). Filtered water samples were stored at −20℃ in a freezer until further laboratory analysis. The NH_4^+ concentration was analyzed onboard immediately after sampling using an INESA N2 Visible Spectrophotometer (Yidianfenxi, Shanghai, China). Other nutrients were analyzed using a continuous flow analyzer (Skalar Analytical, Breda, The Netherlands) following a method reported by Wallerstein and Liebezeit (2009). The detection limits were 0.1 μmol·L^{-1} for nitrate and nitrite, 0.1 μmol·L^{-1} for silicate, and 0.03 μmol·L^{-1} for phosphate. Analytical precision was approximately ±4% for NH_4^+, ±2% for NO_3^-, NO_2^-, and PO_4^{3-}, and ±2.5% for $Si(OH)_4$.

2.3 Pigment analysis

Seawater (3–4 L) was filtered through GF/F filters (0.7 μmol·L^{-1}, Whatman, New Castle, USA) under a gentle vacuum (< 0.5 atm) and dim light conditions. The filters were then stored at −80℃ in a freezer until laboratory analysis. In the laboratory, pigment samples were extracted with 3 mL of 100% high-performance liquid chromatography-grade acetone, ultrasonicated in an ice bath, and stored at −20℃ in a freezer for 2 h. The extract was filtered through a 0.22-μmol·L^{-1} syringe filter (PTFE, Whatman, UK), dried under a gentle N_2 stream, and re-dissolved in a 300-μL mixture of methanol and water (9:1 v/v) before injection. All extraction processes were performed under low light conditions (Feng et al., 2021).

Pigment analysis was conducted on an Ultra Performance Liquid Chromatography (UPLC) system (Acquity H-Class, Waters Corp., Milford, USA) equipped with a C18 column (50×2.1 mm^2 i.d., 1.7 μmol·L^{-1}, Acquity UPLC® BEH), PDAeλ detector, and FLR detector (excitation set at 440 nm and emission set at 660 nm). A binary gradient elution program was used according to Feng et al. (2021), modified from Zapata et al. (2020). The qualitative and quantitative examinations of pigments were based on the retention time, absorption spectra, and area of the peaks in each sample chromatogram (at 440 nm and 660 nm) compared with those of authentic standards. All the pigment standards (chlorophyll-*a* (Chl-*a*), chlorophyll *b* (Chl-*b*), chlorophyll c_3 (Chl-c_3), pheophytin *a* (Phytin-*a*), pheophorbide *a* (Phide-*a*), alloxanthin (Allo), 19′-hexanoyloxyfucoxanthin (Hex-fuco), fucoxanthin (Fuco), peridinin (Peri), violaxanthin (Vio), alloxanthin (Allo), and lutein) used in this study were purchased from DHI Water and Environment (Hørsholm, Denmark). The precision and detection limits of the method were 0.26 μg·L^{-1} and 2.2 μg·L^{-1}, respectively.

2.4 Estimating the phytoplankton community

The CHEMTAX program (Version 1.95) developed by Wright et al. (2009), using eight diagnostic pigments (Table 2) to characterize the phytoplankton community, was used to estimate the relative proportions of different algal types to the total Chl-*a* concentration. Detailed information on the use of the CHEMTAX program in the Amundsen Sea has been reported in Alderkamp et al. (2012). Briefly, as the pigment matrix of phytoplankton is usually affected by environmental conditions (such as irradiance and the nutrient level) (Barlow et al., 2008), a gap usually occurs between the initial matrix and the actual value of the target study area. The final matrix was obtained after 60 successive runs of CHEMTAX and was considered to be

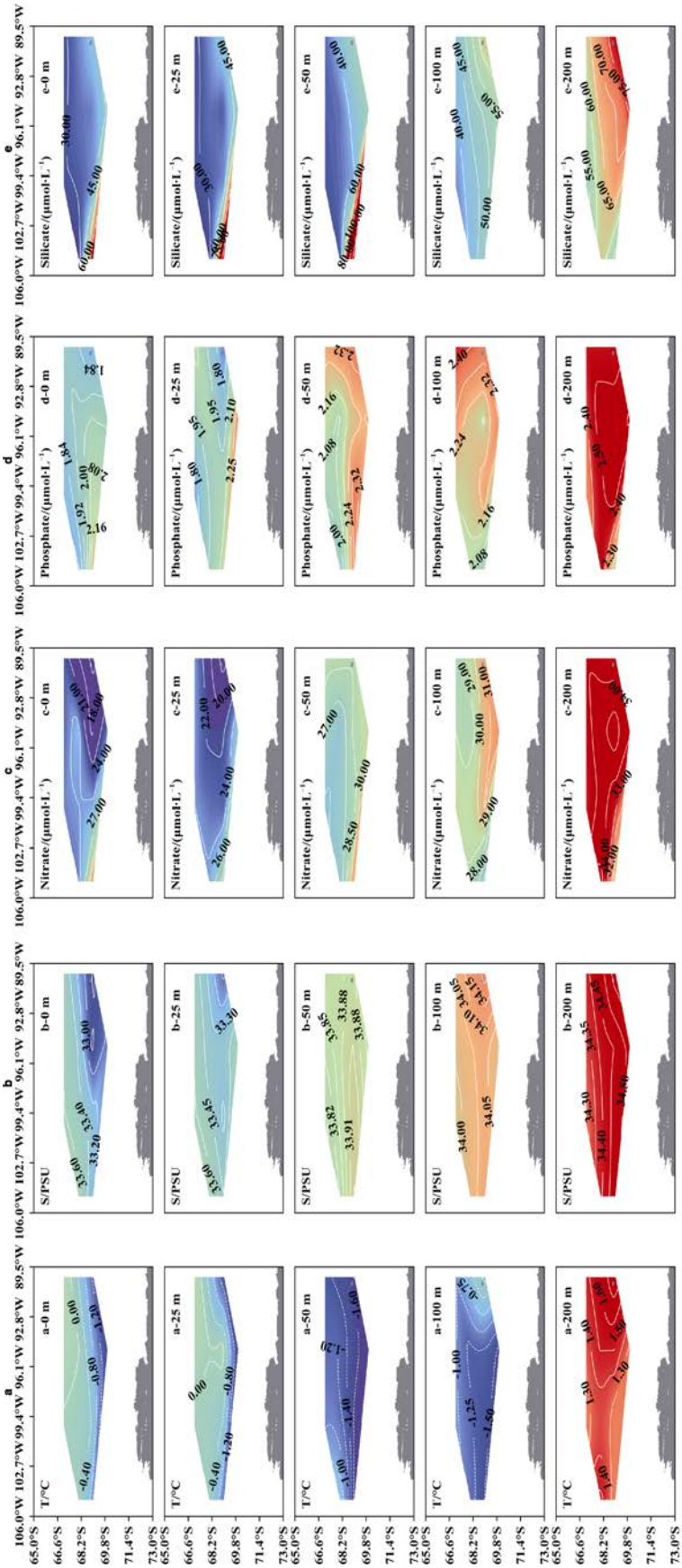

Figure 2 Spatial distributions of temperature (**a**), salinity (**b**), nitrate (**c**), phosphate (**d**), and silicate (**e**).

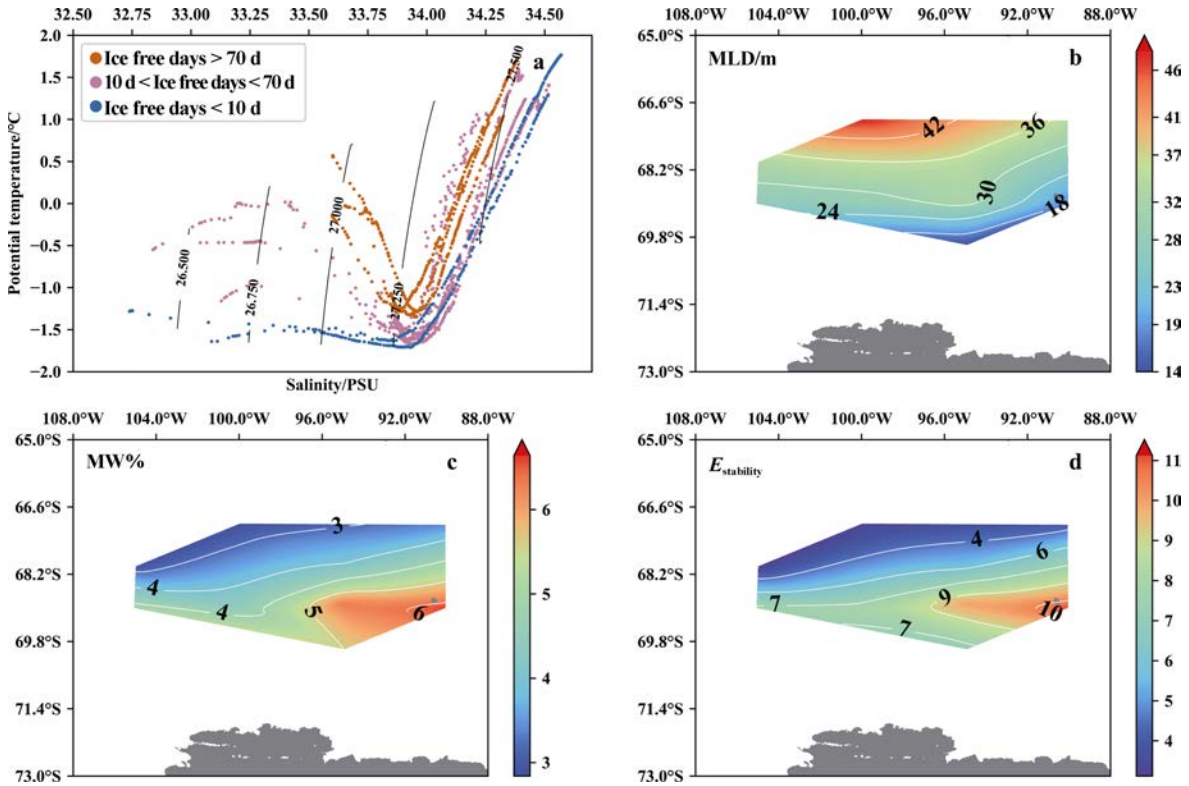

Figure 3 Oceanographic and hydrological characteristics of the study area. The *T*–*S* diagram of the study area (0–200 m) (**a**) (Time lag: time between sampling and sea ice melting; the gray curve indicates the contours of potential density, σ/kg·m^{-3}); distributions of the mixed layer depth (MLD) (**b**); the sea ice melt water percentage (MW%) (**c**) and water column stability ($E_{stability}$) (**d**).

Table 2 Ratios of concentrations of diagnostic pigments to Chl-*a* used for CHEMTAX analysis (Alderkamp et al., 2012)

		Chl-c_3	Peri	Fuco	Vio	Hex-fuco	Allo	Lutein	Chl-*b*	Chl-*a*
(a) Input matrix	Chlorophytes	0.00	0.00	0.00	0.03	0.00	0.00	0.22	0.18	1.00
	Cryptophytes	0.00	0.00	0.00	0.00	0.00	0.22	0.00	0.00	1.00
	Diatoms-A	0.00	0.00	0.57	0.00	0.00	0.00	0.00	0.00	1.00
	Diatoms-B	0.03	0.00	1.02	0.00	0.00	0.00	0.00	0.00	1.00
	Dinoflagellates	0.00	0.54	0.00	0.00	0.00	0.00	0.00	0.00	1.00
	P. antarctica (high Fe)	0.13	0.00	0.08	0.00	0.40	0.00	0.00	0.00	1.00
	P. antarctica (low Fe)	0.27	0.00	0.02	0.00	1.10	0.00	0.00	0.00	1.00
(b) Output matrix	Chlorophytes	0.00	0.00	0.00	0.06	0.00	0.00	0.15	0.17	1.00
	Cryptophytes	0.00	0.00	0.00	0.00	0.00	0.28	0.00	0.00	1.00
	Diatoms-A	0.00	0.00	0.75	0.00	0.00	0.00	0.00	0.00	1.00
	Diatoms-B	0.04	0.00	1.08	0.00	0.00	0.00	0.00	0.00	1.00
	Dinoflagellates	0.00	0.64	0.00	0.00	0.00	0.00	0.00	0.00	1.00
	P. antarctica (high Fe)	0.10	0.00	0.10	0.00	0.43	0.00	0.00	0.00	1.00
	P. antarctica (low Fe)	0.21	0.00	0.02	0.00	1.36	0.00	0.00	0.00	1.00

Notes: Initial ratios before analysis (a) and optimized ratios after analysis (b). Chl-c_3: chlorophyll c_3; Peri: peridinin; Fuco: fucoxanthin; Vio: violaxanthin; Hex-fuco: 19′-hexanoyloxyfucoxanthin; Allo: alloxanthin; Chl-*b*: chlorophyll *b*, and Chl-*a*: chlorophyll *a*.

the real pigment–algae matrix of the study area. The initial input and final matrix pigment ratios for the seven phytoplankton groups are shown in Table 2. Diatoms containing different pigment compositions were divided into two groups; Diatoms-A were represented by *Fragilariopsis* spp., *Chaetoceros* spp., and *Proboscia* spp. (Lee et al., 2016), and Diatoms-B were represented by *Pseudo-nitzschia* spp. (Wright et al., 2010). *P. antarctica* were also divided into two groups (*P. antarctica* [high Fe] and *P. antarctica* [low Fe]) based on the differences in the proportions of Chl-c_3, Peri, and Hex-Fuco to Chl-*a* concentrations and their responses to the dissolved Fe contents (Wright et al., 2010; Alderkamp et al., 2012).

2.5 Integrated values of Chl-*a* and diagnostic pigments

The water column integral pigment concentrations (Chl-*a* and degradation products and diagnostic pigments) were calculated in order to explore the spatial characteristics of phytoplankton biomass. This would overcome the statistical error caused by the analysis of non-equal sampling depths (Zhuang et al., 2014) and the formula was modified for describing the integrated value more correctly. The integrated pigment concentrations in the water column at each station were calculated by Eq. (1):

$$C_{\text{int}} = [C_1(D_1 + D_2) + C_2(D_3 - D_1) + \cdots + C_{n-1}(D_n - D_{n-2}) + C_n(D_n - D_{n-1})]/2 \quad (1)$$

where D_n is the measured depth of a layer and C_n is the concentration in this layer.

2.6 Remote sensing data and physical measurements of seawater properties

The sea ice concentration data (30 km × 30 km) measured by remote sensing were obtained from the sea ice database of the University of Bremen (http://seaice.uni-bremen.de/databrowser/). The sea ice melting date was defined as the date when the sea ice concentration at the station was less than 10%. Time lag (T_{lag}) was determined by the interval between sampling and sea ice melting date.

Based on the in-situ potential temperature, salinity, and pressure data, the potential density of seawater (ρ, kg·m^{-3}) was calculated. The mixed layer depth (MLD) of the water column was calculated based on the depth of the maximum water column buoyancy frequency, and max. (N^2) (Carvalho et al., 2016) following Eq. (2):

$$N^2 = -\frac{g}{\rho}\frac{\partial \rho}{\partial z} \ (\text{rad}^2\cdot\text{s}^{-2}), \quad (2)$$

where g and z represent gravity and the water depth, respectively. The water column stability ($E_{\text{stability}}$) was calculated according to Eq. (3):

$$E_{\text{stability}} = \frac{N^2}{g} \ (10^{-6} \ \text{rad}^2\cdot\text{m}^{-1}), \quad (3)$$

According to former studies, average values of $E_{\text{stability}}$ between 0 and 100 m are considered to represent the horizontal stability of the water column at each station (Mendes et al., 2018). Moreover, according to the methods of Costa et al. (2020) and Mendes et al. (2018), the sea ice melt water percentage (MW%) was calculated as the salinity difference between surface water (S_{surface}) and deep water (S_{deep}, approximately 200 m, which was assumed not to be influenced by sea ice dilution, and the salinity of sea ice was set as 6‰ (Ackley et al., 1979)) in order to evaluate the contribution and dispersal of sea ice melt water. The equation is shown below:

$$\text{MW\%} = \left(1 - \frac{S_{\text{surface}} - 6}{S_{\text{deep}} - 6}\right) \times 100, \quad (4).$$

2.7 Statistical analysis

Redundancy analysis (RDA) using the 'vegan' package (Oksanen et al., 2013) was used to determine relationships between measured parameters. The significance of the RDA was evaluated by Monte-Carlo tests. Pearson correlation analysis and a two-tailed test of significance were performed using SPSS 20 (Chicago, IL, USA) to determine the relationships between the measured parameters.

3 Results

3.1 Hydrology

Water masses in the eastern Amundsen Sea are influenced by the eastward flow of water currents (e.g., the Antarctic circumpolar current (ACC)) (Figure 1) (Jacobs and Comiso, 1997; Walker et al., 2013). Most of the study stations were located north of the southern boundary of ACC; only stations A8-07 and A9-08 were located close to the ice-edge line (Figure 1). During the sampling period, temperature (mean: −0.65±1.02℃) and salinity (mean: 33.9±0.4) ranged from −1.7℃ to 1.8℃ and from 32.77 to 34.58, respectively (Figures 2 and 3). The lowest temperature was found at the depth of 75 m at station A8-07, and the highest temperature was found at 200 m at station A9-08. The lowest salinity value was found in the surface layers of stations A8-08 and A9-08. Spatially, in the water column above 25 m depth, the temperature and salinity increased northward and northwestward, respectively, while both were fairly uniform below 50 m (Figure 2). Vertically, the temperature and salinity of the water column showed different variation trends due to the influence of sea ice melt water input (Figures 3 and 4). Generally, the temperature was fairly uniform in the upper layers and decreased markedly near the thermocline and then increased with greater water depth, while the salinity generally increased with increasing water depth with a halocline occurring near the MLD (Figures 3 and 4).

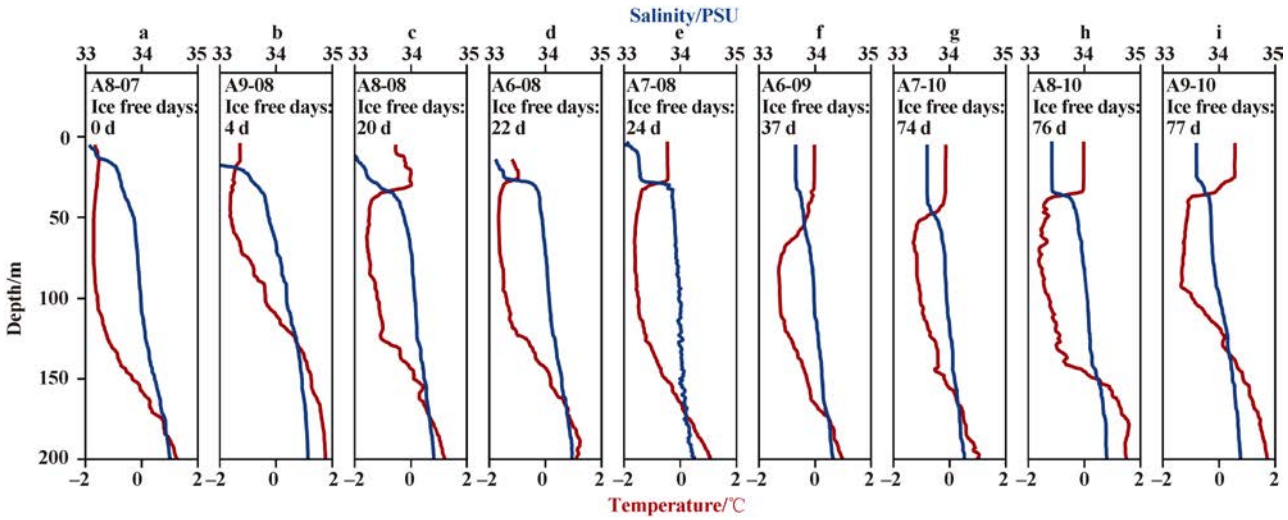

Figure 4 Vertical of profiles of salinity (blue lines) and temperature (red lines) measured at typical stations in the study area (Ice free days increased toward the right).

The MLD of the study area ranged from 14 m (station A8-07) to 48 m (station A7-10) with an average of 30±9 m. As shown in Figure 3b, the region with deeper MLD was located in the northern part of the study area, while shallower MLD was found in the region near the ice-edge line (Figure 3b). MW% ranged from 2.9% to 6.6%, with an average of 4.6%±1.3%, and generally increased southward (Figure 3c). The $E_{stability}$ ranged from 3.1 to 11.1, with an average of 6.6±2.6, and generally showed a similar distribution pattern to that of MW% (r=0.91, p<0.05) (Figure 3d), with the highest and lowest values obtained at stations A9-08 and A6-09, respectively.

3.2 Regional oceanography characteristics

The study area is mainly located in the slope region of the eastern Amundsen Sea, and the water properties and stratification are influenced by the ACC and seasonal sea ice cover. Due to the different distances to the ice-edge line and the retreat of sea ice, different stations had different hydrological characteristics (Figure 4). The stations near the ice-edge line (A8-07 and A9-08) had a shorter T_{lag} between the sampling date and the date of the complete melting of sea ice (Table 1). In most stations with T_{lag} shorter than 10 d, the water in the upper layers was characterized by considerably low temperature and salinity (Figures 3a, 4a and 4b), wider salinity variable ranges, and higher MW% (5.6% and 6.6% for stations A8-07 and A9-08, respectively) (Figure 3c). These phenomena contributed to a shallower MLD, and higher $E_{stability}$ therein (Figure 3). Compared to stations near the ice-edge line, the water column of other stations (A6-09, A7-10, and A9-10) with a longer T_{lag} (e.g., longer than one month) had much lower MW% (~3%) and was significantly influenced by the eastward-flowing ACC, all showed characteristics of higher temperature and salinity (Figure 2). The difference in salinity and temperature between the upper and lower water columns was much smaller (Figure 4), but with a marked thermocline and halocline at approximately 50 m (Figures 4h and 4i). These phenomena further resulted in thorough water mixing characterized by deeper MLD (> 33 m) and lower $E_{stability}$ (<4.1) (Figure 3). The CDW with high temperature and salinity has been reported at depths of 300–500 m (Turner et al., 2017). However, strong signals of CDW were observed at a depth of approximately 150 m in the northern stations of the study area, likely due to strong turbulence mixing (Figures 4h and 4i).

3.3 Nutrient concentrations and ratios

The average concentrations of NO_3^-, NO_2^-, NH_4^+, PO_4^{3-}, and $Si(OH)_4$ were 27.6±4.4 μmol·L^{-1} (approximately 13.7–35.7 μmol·L^{-1}), 0.2±0.1 μmol·L^{-1} (approximately 0–0.6 μmol·L^{-1}), 0.8±0.4 μmol·L^{-1} (approximately 0.1–1.9 μmol·L^{-1}), 2.2±0.3 μmol·L^{-1} (approximately 0.7–2.6 μmol·L^{-1}), and 53.0±24.9 μmol·L^{-1} (approximately 24.4–141.5 μmol·L^{-1}), respectively. Due to the lower concentrations of NO_2^- and NH_4^+ in the study area, only NO_3^- was discussed in this study. As shown in Figure 2, in the water column above 100 m depth, the nutrient concentrations showed an increasing trend with higher latitude, while nutrient concentrations were fairly spatially uniform in the deeper water layer. Vertically, nutrient concentrations showed an increasing trend with increasing water depth (Figure 2). With respect to the nutrient compositions, the N/P ratios ranged from 7.8–39.2, with an average of 13.0±3.5, the Si/P ratios ranged from 12.9–61.3, with an average of 24.6±11.1, and the N/Si ratio ranged from 0.2–1.0, with an average of 0.6±0.2. According to the potential stoichiometric criteria for algal physiology ($Si(OH)_4$ > 2 μmol·L^{-1}, NO_3^- > 1 μmol·L^{-1}, PO_4^{3-} > 0.1 μmol·L^{-1}, 10 < N/P ratio < 22, and Si/P ratio > 10) (Justic et al., 1995), the nutrient concentrations in study area were generally high and no potential nutrient limitation occurred; only the N/P ratios of the surface layers of

stations A9-08 (8.7) and A8-08 (7.8) were lower than 10.

3.4 Concentrations and distribution of integrated pigments

Concentrations of integrated Chl-*a* (above 200 m) ranged from 21.4 mg·m^{-2} to 148.4 mg·m^{-2}, with an average of 35.7± 53.4 mg·m^{-2}; the lowest value was recorded at station A7-08 and the highest at station A9-08 (Figure 5a). The concentrations of phide-*a* (average 33.6±16.9 mg·m^{-2}) were much higher than those of Phytin-*a* (average 5.7±3.0 mg·m^{-2}), with the lowest values at station A9-10 (below the detection limitation) and the highest values at station A9-08 (111.7 mg·m^{-2} and 16.1 mg·m^{-2} for Phide-*a* and Phytin-*a*, respectively) (Figures 5b and 5c). The concentration of Phide-*a* was significantly correlated with those of Chl-*a* (r=0.62, p<0.01) and Phytin-*a* (r=0.83, p<0.01). At most of the stations, the concentrations of Chl-*a* and its degradation products showed decreasing trends with increasing water column depths, while certain stations showed constant profiles in the upper 100 m depth (Figure 6).

Among the diagnostic pigments, the Hex–Fuco(23.0±18.7 mg·m^{-2}), Fuco (14.6±24.1 mg·m^{-2}), and Peri (3.7±6.4 mg·m^{-2}) pigments were abundant, while the concentrations of other diagnostic pigments such as Allo (0.8±1.2 mg·m^{-2}), Chl-*b* (1.7±1.9 mg·m^{-2}), and Vio (0.9±1.0 mg·m^{-2}) were fairly low in this study. As shown in Figure 5, the spatial distributions of the integrated Chl-*a* showed a patchy distribution pattern, with the highest concentrations found in the area near Peter I Island, and the lowest value was measured in the center of the study area. Most of the abundant diagnostic pigments (Fuco, Peri, and Allo) showed similar spatial distributions to that of Chl-*a* (Figure 5a). In contrast, other diagnostic pigments (Hex-Fuco and Ch-*b*) generally showed similar distribution patterns to that of the degradation products of Chl-*a*.

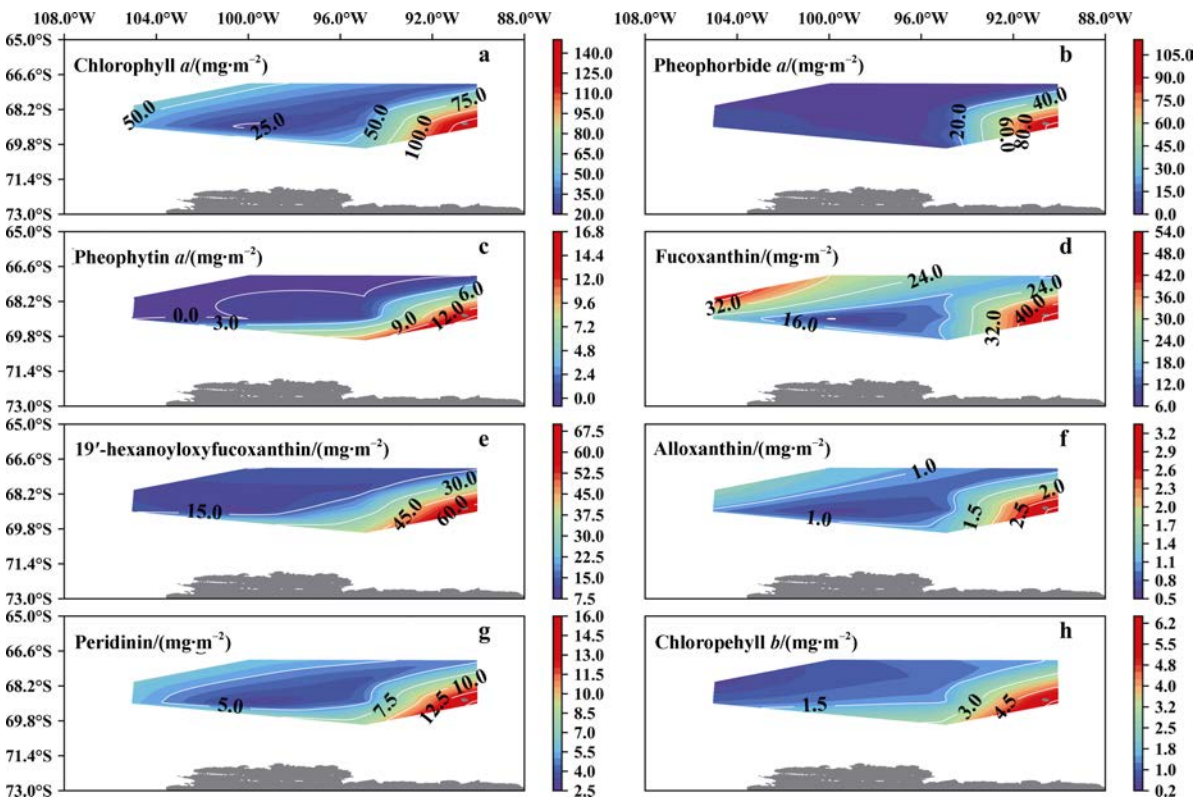

Figure 5 Spatial distributions of the integrated concentrations of Chl-*a* (**a**), degradation products (**b**–**c**) and diagnostic pigments (**d**–**h**).

3.5 Phytoplankton community structure based on CHEMTAX

The phytoplankton community determined by the CHEMTAX model is shown in Figure 7. Briefly, Diatoms-B (29%±18%) and *P. antarctica* (low Fe) (22%±13%) were the two dominant phytoplankton groups, and their relative abundances ranged from 0 to 65% and from 0 to 56%, respectively. Spatially, the Diatoms-B were more concentrated in the northwest of the study area, while the *P. antarctica* (low Fe) showed a decreasing trend northward (Figure 7). By contrast, the contributions of Dinoflagellates, Chlorophytes, Cryptophytes, *P. antarctica* (high Fe), and Diatoms-A to the phytoplankton community were lower and contributed approximately 17%±8% (0–54%), 15%±13% (1%–61%), 9%±6% (0–44%), 5%±9% (0–45%), and 3%±7% (0–33%). The proportions of *P. antarctica* (high Fe) and Diatoms-A generally showed respective low and high values in the center of the study area (Figures 7c and 7a). The other groups of phytoplankton showed no obvious distribution patterns. Vertically, the percentages of Diatoms-B and Dinoflagellates generally

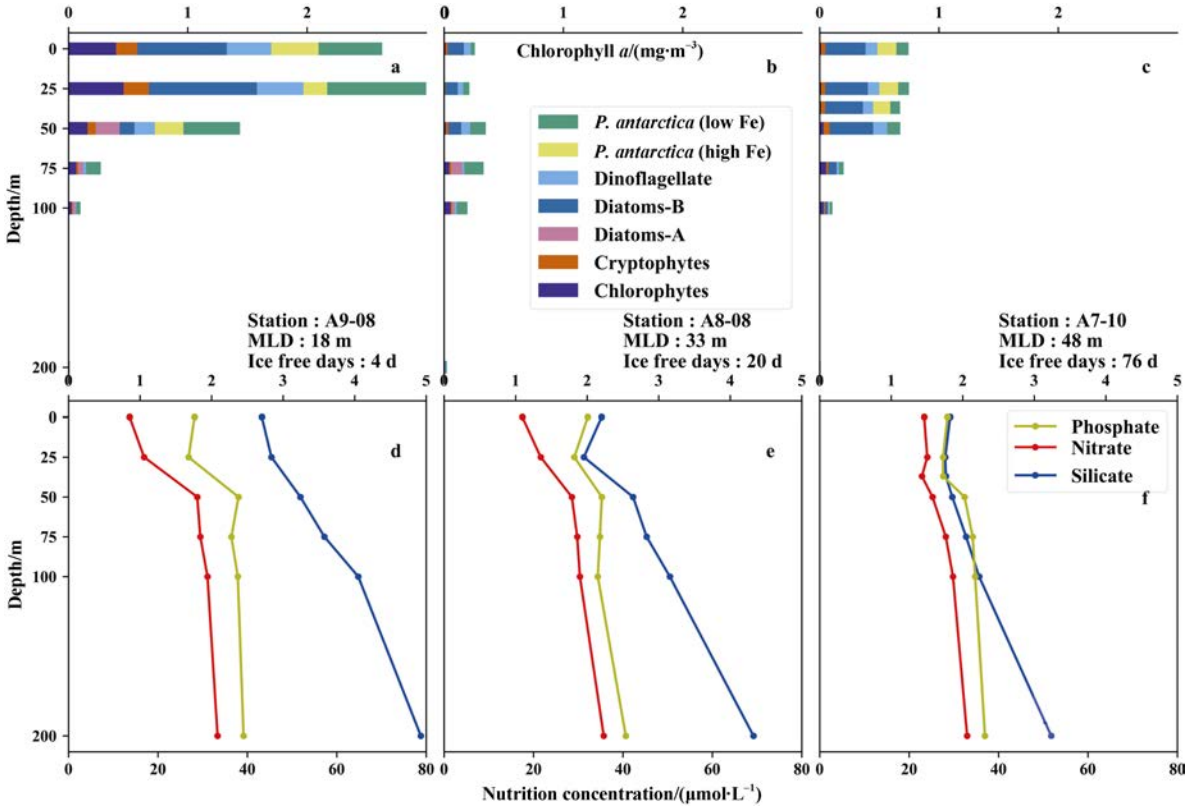

Figure 6 Vertical profiles of the phytoplankton community structure and nutrient compositions at three typical stations (**a**, **d**: A9-08; **b**, **e**: A8-08; **c**, **f**: A7-10).

showed decreasing trends with greater water depth (r=0.63 and 0.27, p<0.05, Figure 8), while the proportions of Chlorophytes and Cryptophytes showed increasing trends downward (r=−0.63 and −0.27, respectively, p<0.05, Figure 8).

4 Discussion

4.1 Influence of nutrient status on phytoplankton growth

As the Southern Ocean is a typical high nutrient, low chlorophyll region, our study area also had abundant macronutrients, such as nitrate, phosphate, and silicate (Figure 2), and no potential nutrient limitation occurred according to the potential stoichiometric criteria for algal physiology ($Si(OH)_4$ >2 μmol·L^{-1}, NO_3^- >1 μmol·L^{-1}, PO_4^{3-} > 0.1 μmol·L^{-1}, 10 < N/P ratio < 22, and Si/P ratio > 10) (Justic et al., 1995). A negative relationship was observed between the Chl-*a* concentration and nitrate and phosphate concentrations (r=−0.59, p<0.01 and r=−0.38, p<0.01, respectively), indicating the efficient consumption of macronutrients by phytoplankton. Moreover, different types of phytoplankton showed different relationships with different nutrient compositions due to their varying absorption capacity and tolerance to nutrient compositions and concentrations. For example, the proportion of Diatoms-B was negatively correlated with Si/N (r=−0.39, p<0.05, Figure 8), and the proportion of *P. antarctica* (low Fe) was positively correlated with concentrations of PO_4^{3-} (r=0.28, p<0.05).

The water masses and currents could affect phytoplankton biomass and the community structure by mediating the supply of nutrients (especially the micronutrient Fe) in the water column (Alderkamp et al., 2012). In the open area of the Southern Ocean, the dissolved Fe concentration is only 0.04 nmol·L^{-1} (Sanudo-Wilhelmy et al., 2002), and it is even lower in the ACC (approximately 0.01 nmol·L^{-1}) (Planquette et al., 2013). Thus, the limited supply of bio-available dissolved Fe is considered a limiting factor for phytoplankton growth in the Southern Ocean (Moore et al., 2007). In this study, *P. antarctica* (low Fe) (22%±13%), which is typically found in Fe-limited environments, was the second highest group in the phytoplankton community, a finding that is consistent with the previous study by Alderkamp et al. (2012). The widely distributed *P. antarctica* (low Fe) indicated that the Fe supply of the study area is generally low (Figure 7d). By contrast, there were high proportions of *P. antarctica* (high Fe) in the southeastern and northwestern parts of the study area (Figure 7c), indicating potential Fe sources in these areas. The input of dissolved Fe from sea ice melt has been

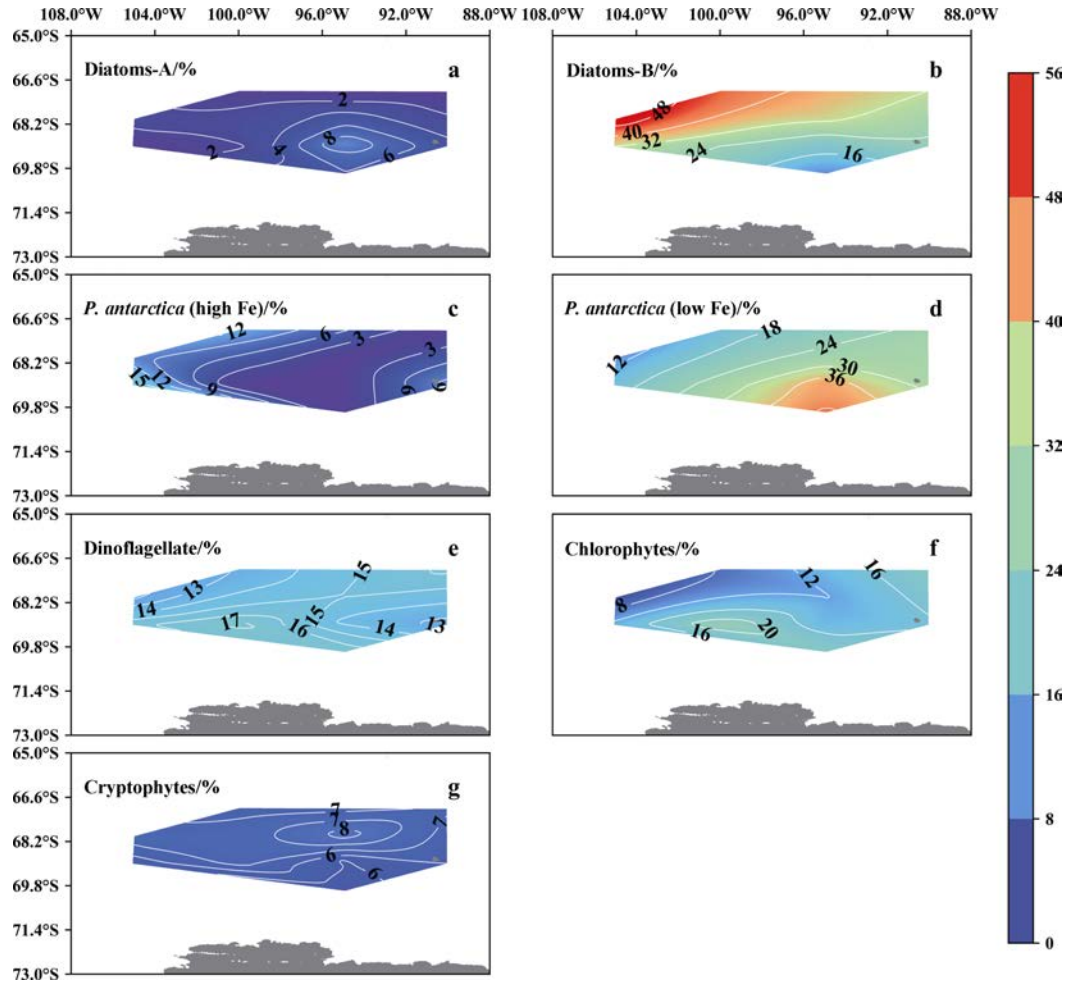

Figure 7 Spatial distribution of proportions of different phytoplankton groups in the phytoplankton community calculated from CHEMTAX calculations.

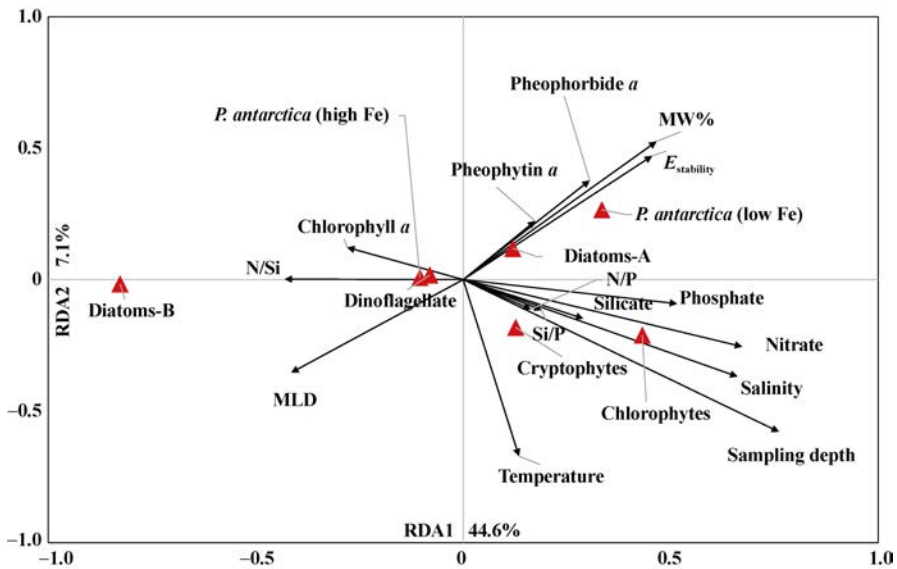

Figure 8 Redundancy analysis (RDA) ordination plot for the first two principal dimensions of the relationships between the phytoplankton stock and community structure with environmental parameters. Arrows indicate environmental variables. Red triangles refer to absolute contributions of phytoplankton groups.

proven to be a major Fe source in the ice-edge region (Raiswell et al., 2008), such as the high dissolved Fe concentrations (as high as ~1.31 nmol·L^{-1}) observed near Pine Island Glacier (Gerringa et al., 2012). We speculated that an efficient supply of ice-sourced dissolved Fe at the stations with higher MW% (r=0.76, p<0.05) and shorter T_{lag} near the ice-edge line was the major reason for the high phytoplankton biomass therein (Figures 3 and 5). Correspondingly, lower macronutrient concentrations were observed in the southeastern part of the study area, indicating efficient consumption of macronutrients by phytoplankton (Figure 2). Despite the low MW% in the northern region of the study area (Figure 3c), high phytoplankton biomass and a high proportion of Diatoms-B were observed (Figures 5a and 7b), suggesting a potential source of dissolved Fe input. The upwelling and intrusion of dissolved Fe concentrated in CDW (as high as 0.3 nmol·L^{-1}) (Sherrell et al., 2015), as suggested by the high temperature water mass found at 150 m in stations A6-09, A8-09, and A9-10 (Figure 6), may be an important Fe source. For example, Fragoso et al. (2012) reported an algal bloom event dominated by *P. antarctica* bloom, caused by the intrusion of CDW in the Ross Sea. Additionally, due to the weak water column stability (Figure 3e), turbulent mixing could vertically deliver the dissolved Fe from CDW to the upper layers (Sherrell et al., 2015), finally leading to high Chl-*a* concentrations (Figure 5a) and a constant Chl-*a* vertical profile without a deep chlorophyll maximum layer (as in station A7-10, Figure 6c).

4.2 Effect of water mixing and stability on the phytoplankton community

The stability of the water column in the euphotic layer influenced by water mass mixing is one of the most important factors dominating phytoplankton and zooplankton activities in the continental marginal sea of the Southern Ocean (Mendes et al., 2012; Mendes et al., 2018; Feng et al., 2021). In this study, positive relationships were observed between $E_{stability}$ and Chl-*a* (r=0.64, p<0.05) and Phide-*a* (r=0.78, p<0.05) concentrations (Figure 8). Similarly, Garcia-Munoz et al. (2013) reported that well-stratified water column favors phytoplankton growth. Taking station A9-08 as an example, this station had the highest MW% (~6.6%) and $E_{stability}$ (~11) and the second-shallowest MLD (~18 m) due to its shortest T_{lag} (~4 d). The well-stratified water column and efficient dissolved Fe supply sourced from melting sea ice led to the highest phytoplankton biomass (Boyd et al., 2012) and diverse phytoplankton composition therein, and Diatoms-B, Dinoflagellates, Chlorophytes, and *P. antarctica* (high Fe) all contributed significantly to the phytoplankton community (Figure 6). Additionally, due to the rapidly changing water properties and decreasing light availability with greater water depth, the phytoplankton biomass and the proportion of diatoms decreased significantly (Figure 6a). Conversely, at the stations with long T_{lag} (~20 d) and deep MLD (including A8-08, MLD=33 m, Figure 6b), strong water mixing would limit the growth of phytoplankton, favoring stable hydrodynamic conditions. At these stations, the biomass was low and constant, and the phytoplankton community changed from Diatoms-B- dominated in the upper 50 m to *P. antarctica* (low Fe)-dominated in the lower water layers (Figure 6b). Moreover, in the northern part of the study area (e.g., station A7-10), despite a much deeper MLD (~48 m) and the lowest $E_{stability}$ (~3), the phytoplankton community was still dominated by Diatoms-B. This was probably due to the supply of bio-available Fe from the upwelling and intrusion of CDW (Figures 4g–4i).

Compared to diatoms, *P. antarctica* is much more adapted to environments with shallow MLD and strong light intensity (Alderkamp et al., 2012; Wolf et al., 2013). In this study, the MLD and $E_{stability}$ were significantly influenced by MW% and were negatively (r=−0.72, p<0.05) and positively (r=0.91, p<0.05) correlated, respectively, with MW% (Figure 8). Correspondingly, with respect to the two dominated phytoplankton groups, the proportion of Diatoms-B (r=−0.82, p<0.01) and *P. antarctica* (low Fe) (r=0.69, p<0.05) showed significant relationships with MW%. As the dominant group of the phytoplankton community in the sea ice (Arrigo et al., 2014), the seeding effects of *P. antarctica* due to sea ice melting contributed significantly to the phytoplankton community in the water column of the ice-edge region (>30% in this study). Moreover, consistent with former studies (in the western part of the Amundsen Sea, the Antarctic Peninsula, and the Ross Sea) (Alderkamp et al., 2012; Mendes et al., 2013; Nunes et al., 2019), Diatoms-A (*Fragilariopsis* spp., *Chaetoceros* spp., and *Proboscia* spp.) were more adapted to environments with shallow MLD contrast to Diatoms-B (such as the ice-edge region, Figure 7a), due to a stronger heat absorption capacity compared to other algae (Villafañe et al., 2008; Kropuenske et al., 2010). Thus, Diatoms-A showed a positive relationship with MW% (r=0.66, p<0.05). Conversely, Diatoms-B favored environments with deep MLD and have been reported as dominant species in the Atlantic and Pacific Ocean sectors of the Southern Ocean (Sun et al., 2003; Kopczynska et al., 2007; Mendes et al., 2018). Generally, the competitive position of *P. antarctica* and diatoms in the study area were dominated by the water stability, which is highly influenced by the input of sea ice melt water and water mass mixing.

As zooplankton (such as krill) prefer to live in shallow water depths with a stable water column, environments with shallow MLD and high $E_{stability}$ caused by strong sea ice melt water input would be favored by zooplankton (Davidson et al., 2010; Jarvis et al., 2010). Phytin-*a* and Phide-*a* are considered as products of the feeding activity of large zooplankton (krill and copepods) and smaller

zooplankton (protozoa) (Jeffrey et al., 1997). In this study, the MW% and concentrations of Phytin-*a* and Phide-*a* showed similar distribution patterns, indicating strong feeding activities in the ice-edge region (Figures 3c, 5b and 5c). The Phytin-*a* concentration and the proportion of Diatoms-B had a significantly negative relationship (r=−0.29, p<0.01), further indicating the diatoms were the favorite food source for large zooplankton such as krill in the ice-edge region.

5 Conclusion

In the eastern part of the Amundsen Sea, the water properties are influenced by the ACC, CDW, and seasonal sea ice cover. The water masses and current affected the phytoplankton biomass and community structure by mediating the supply of nutrients (especially the micronutrient Fe) and the water stability. In the ice-edge region, the input of sea ice melt water provided bio-available dissolved Fe and promoted the stratification of the water column, resulting in a shallow MLD and high water stability. This favored the growth of *P*. *antarctica* and resulted in high phytoplankton biomass, active zooplankton feeding activities, and a diverse phytoplankton composition (Diatoms-B, Dinoflagellates, Chlorophytes, and *P*. *antarctica* (high Fe) all contributed significantly to the phytoplankton community). Additionally, due to the rapidly changing water properties and decreasing light availability with greater water depth, the phytoplankton biomass and diatom proportion decreased significantly. In the northern part of the study area, the stations with low sea ice melt water contributions were markedly influenced by turbulence mixing and CDW upwelling and were characterized by deep MLD and low water stability. Although strong water mixing would limit the growth of phytoplankton, due to the supply of bio- available Fe from upwelling and the intrusion of CDW, the biomass was still high, and the phytoplankton community was still dominated by Diatoms-B. Conversely, in the center of the study area, due to the long T_{lag} and weak intrusion of CDW, the biomass was low and constant, and the phytoplankton community changed from Diatoms-B-dominated to *P*. *antarctica* (low Fe)-dominated with greater water depth. This study improves the understanding of phytoplankton dynamics in rapidly changing environments of the Antarctic continental marginal seas.

Acknowledgments This study was financially supported by National Polar Special Program “Impact and Response of Antarctic Seas to Climate Change” (Grant nos. IRASCC 02-02, 01-01-02), was supported by the National Natural Science Foundation of China (Grant nos. 41976228, 41976227, 41506223), and the Scientific Research Fund of the Second Institute of Oceanography, MNR (Grant nos. JG1805, JG2011, JG2013). We thank the crew members of the 35th CHINARE for their sampling assistance and the Physical Oceanography Group of this cruise for providing hydrological data. We would like to thank two anonymous reviewers, and Guest Editor Dr. Jianfeng He, for their valuable suggestions and comments that improved this article.

References

Ackley S F, Buck K R, Taguchi S. 1979. Standing crop of algae in the sea ice of the Weddell Sea region. Deep Sea Res A Oceanogr Res Pap, 26(3): 269-281, doi:10.1016/0198-0149(79)90024-4.

Ainley D G, Clarke E D, Arrigo K, et al. 2005. Decadal-scale changes in the climate and biota of the Pacific sector of the Southern Ocean, 1950s to the 1990s. Antarct Sci, 17(2): 171-182, doi:10.1017/s0954102005002567.

Alderkamp A C, Mills M M, van Dijken G L, et al. 2012. Iron from melting glaciers fuels phytoplankton blooms in the Amundsen Sea (Southern Ocean): Phytoplankton characteristics and productivity. Deep Sea Res Part II: Top Stud Oceanogr, 71-76: 32-48, doi:10.1016/j.dsr2.2012.03.005.

Arrigo K R, Brown Z W, Mills M M. 2014. Sea ice algal biomass and physiology in the Amundsen Sea, Antarctica. Elem: Sci Anthropocene, 2: 000028, doi:10.12952/journal.elementa.000028.

Arrigo K R, van Dijken G L. 2003. Phytoplankton dynamics within 37 Antarctic coastal polynya systems. J Geophys Res, 108 (C8): 3271, doi: 10.1029/2002JC001739.

Barlow R, Kyewalyanga M, Sessions H, et al. 2008. Phytoplankton pigments, functional types, and absorption properties in the Delagoa and Natal bights of the Agulhas ecosystem. Estuar Coast Shelf Sci, 80(2): 201-211, doi:10.1016/j.ecss.2008.07.022.

Boyd P W, Arrigo K R, Strzepek R, et al. 2012. Mapping phytoplankton iron utilization: Insights into Southern Ocean supply mechanisms. J Geophys Res: Oceans, 117(C6): C06009, doi:10.1029/2011JC007726.

Carvalho F, Kohut J, Oliver M J, et al. 2016. Mixing and phytoplankton dynamics in a submarine canyon in the West Antarctic Peninsula. J Geophys Res: Oceans, 121(7): 5069-5083, doi:10.1002/2016JC011650.

Cavalieri D J, Parkinson C L. 2008. Antarctic sea ice variability and trends, 1979–2006. J Geophys Res: Oceans, 113(C7): C07004, doi:10.1029/2007JC004564.

Cheah W, Soppa M A, Wiegmann S, et al. 2017. Importance of deep mixing and silicic acid in regulating phytoplankton biomass and community in the iron-limited Antarctic Polar Front region in summer. Deep Sea Res Part II: Top Stud Oceanogr, 138: 74-85, doi:10.1016/j.dsr2.2016.05.019.

Costa R R, Mendes C R B, Tavano V M, et al. 2020. Dynamics of an intense diatom bloom in the Northern Antarctic Peninsula, February 2016. Limnol Oceanogr, 65(9): 2056-2075, doi:10.1002/lno.11437.

Davidson A T, Scott F J, Nash G V, et al. 2010. Physical and biological control of protistan community composition, distribution and abundance in the seasonal ice zone of the Southern Ocean between 30 and 80°E. Deep Sea Res Part II: Top Stud Oceanogr, 57(9-10): 828-848, doi:10.1016/j.dsr2.2009.02.011.

Ducklow H W, Schofield O, Vernet M, et al. 2012. Multiscale control of bacterial production by phytoplankton dynamics and sea ice along the western Antarctic Peninsula: a regional and decadal investigation. J Mar Syst, 98-99: 26-39, doi:10.1016/j.jmarsys.2012.03.003.

Feng Y B, Li D, Zhao J, et al. 2021. Environmental drivers of

phytoplankton crops and taxonomic composition in northeastern Antarctic Peninsula adjacent sea area. Acta Oceanol Sin, doi:10.1007/s13131-021-1865-4.

Fragoso G M, Smith Jr. W O. 2012. Influence of hydrography on phytoplankton distribution in the Amundsen and Ross seas, Antarctica. J Mar Syst, 89(1): 19-29, doi:10.1016/j.jmarsys.2011.07.008.

García-Muñoz C, Lubián L M, García C M, et al. 2013. A mesoscale study of phytoplankton assemblages around the South Shetland Islands (Antarctica). Polar Biol, 36(8): 1107-1123, doi:10.1007/s00300-013-1333-5.

Gerringa L J A, Alderkamp A C, Laan P, et al. 2012. Iron from melting glaciers fuels the phytoplankton blooms in Amundsen Sea (Southern Ocean): Iron biogeochemistry. Deep Sea Res Part II: Top Stud Oceanogr, 71-76: 16-31, doi:10.1016/j.dsr2.2012.03.007.

Jacobs S S, Comiso J C. 1997. Climate variability in the Amundsen and bellingshausen seas. J Climate, 10(4): 697-709, doi:10.1175/1520-0442(1997)0102.0.co;2.

Jarvis T, Kelly N, Kawaguchi S, et al. 2010. Acoustic characterisation of the broad-scale distribution and abundance of Antarctic krill (*Euphausia superba*) off East Antarctica (30–80°E) in January–March 2006. Deep Sea Res Part II: Top Stud Oceanogr, 57(9-10): 916-933, doi:10.1016/j.dsr2.2008.06.013.

Justić D, Rabalais N N, Turner R E. 1995. Stoichiometric nutrient balance and origin of coastal eutrophication. Mar Pollut Bull, 30(1): 41-46, doi:10.1016/0025-326X(94)00105-I.

Jeffrey S W, Mantoura R F C, Wright S W. 1997. Phytoplankton pigments in oceanography: guidelines to modem methods. Paris: Unesco Publishing, 1-661, doi:10.1017/S0025315400036389.

Konrad H, Shepherd A, Gilbert L, et al. 2018. Net retreat of Antarctic glacier grounding lines. Nat Geosci, 11(4): 258-262, doi:10.1038/s41561-018-0082-z.

Kopczyńska E E, Savoye N, Dehairs F, et al. 2007. Spring phytoplankton assemblages in the Southern Ocean between Australia and Antarctica. Polar Biol, 31(1): 77-88, doi:10.1007/s00300-007-0335-6.

Kropuenske L R, Mills M M, van Dijken G L, et al. 2010. Strategies and rates of photoacclimation in two major southern ocean phytoplankton taxa: *phaeocystis Antarctica* (haptophyta) and *fragilariopsis cylindrus* (bacillariophyceae). J Phycol, 46(6): 1138-1151, doi:10.1111/j.1529-8817.2010.00922.x.

Landschützer P, Gruber N, Bakker D C E. 2016. Decadal variations and trends of the global ocean carbon sink. Glob Biogeochem Cycles, 30(10): 1396-1417, doi:10.1002/2015GB005359.

Lee Y, Yang E J, Park J, et al. 2016. Physical-biological coupling in the Amundsen Sea, Antarctica: Influence of physical factors on phytoplankton community structure and biomass. Deep Sea Res Part I: Oceanogr Res Pap, 117: 51-60, doi:10.1016/j.dsr.2016.10.001.

Mendes C R B, de Souza M S, Garcia V M T, et al. 2012. Dynamics of phytoplankton communities during late summer around the tip of the Antarctic Peninsula. Deep Sea Res Part I: Oceanogr Res Pap, 65: 1-14, doi:10.1016/j.dsr.2012.03.002.

Mendes C R B, Tavano V M, Kerr R, et al. 2018. Impact of sea ice on the structure of phytoplankton communities in the northern Antarctic Peninsula. Deep Sea Res Part II: Top Stud Oceanogr, 149: 111-123, doi:10.1016/j.dsr2.2017.12.003.

Mendes C R B, Tavano V M, Leal M C, et al. 2013. Shifts in the dominance between diatoms and cryptophytes during three late summers in the Bransfield Strait (Antarctic Peninsula). Polar Biol, 36(4): 537-547, doi:10.1007/s00300-012-1282-4.

Moore C M, Seeyave S, Hickman A E, et al. 2007. Iron-light interactions during the CROZet natural iron bloom and EXport experiment (CROZEX) I: Phytoplankton growth and photophysiology. Deep Sea Res Part II: Top Stud Oceanogr, 54(18-20): 2045-2065, doi:10.1016/j.dsr2.2007.06.011.

Nunes S, Latasa M, Delgado M, et al. 2019. Phytoplankton community structure in contrasting ecosystems of the Southern Ocean: South Georgia, South Orkneys and western Antarctic Peninsula. Deep Sea Res Part I: Oceanogr Res Pap, 151: 103059, doi:10.1016/j.dsr.2019.06.005.

Oksanen J, Blanchet F G, Kindt R, et al. 2013. Package 'vegan'. Community ecology package, version 2.0–9, 1-295.

Petrou K, Kranz S A, Trimborn S, et al. 2016. Southern Ocean phytoplankton physiology in a changing climate. J Plant Physiol, 203: 135-150, doi:10.1016/j.jplph.2016.05.004.

Planquette H, Sherrell R M, Stammerjohn S, et al. 2013. Particulate iron delivery to the water column of the Amundsen Sea, Antarctica. Mar Chem, 153: 15-30, doi:10.1016/j.marchem.2013.04.006.

Pritchard H D, Ligtenberg S R M, Fricker H A, et al. 2012. Antarctic ice-sheet loss driven by basal melting of ice shelves. Nature, 484(7395): 502-505, doi:10.1038/nature10968.

Raiswell R, Benning L G, Tranter M, et al. 2008. Bioavailable iron in the Southern Ocean: the significance of the iceberg conveyor belt. Geochem Trans, 9: 7, doi:10.1186/1467-4866-9-7.

Rignot E, Jacobs S, Mouginot J, et al. 2013. Ice-shelf melting around Antarctica. Science, 341(6143): 266-270, doi:10.1126/science.1235798.

Rost B, Riebesell U. 2004. Coccolithophores and the biological pump: responses to environmental changes//Thierstein H R, Young J R. Coccolithophores. Springer, Berlin, Heidelberg, 99-125, doi:10.1007/978-3-662-06278-4_5.

Sabine C L, Feely R A, Gruber N, et al. 2004. The oceanic sink for anthropogenic CO_2. Science, 305(5682): 367-371, doi:10.1126/science.1097403.

Sañudo-Wilhelmy S A, Olsen K A, Scelfo J M, et al. 2002. Trace metal distributions off the Antarctic Peninsula in the Weddell Sea. Mar Chem, 77(2-3): 157-170, doi:10.1016/S0304-4203(01)00084-6.

Sarthou G, Timmermans K R, Blain S, et al. 2005. Growth physiology and fate of diatoms in the ocean: a review. J Sea Res, 53(1-2): 25-42, doi:10.1016/j.seares.2004.01.007.

Schmidtko S, Heywood K J, Thompson A F, et al. 2014. Multidecadal warming of Antarctic waters. Science, 346(6214): 1227-1231, doi:10.1126/science.1256117.

Schofield O, Saba G, Coleman K, et al. 2017. Decadal variability in coastal phytoplankton community composition in a changing West Antarctic Peninsula. Deep Sea Res Part I: Oceanogr Res Pap, 124: 42-54, doi:10.1016/j.dsr.2017.04.014.

Sherrell R M, Lagerström M E, Forsch K O, et al. 2015. Dynamics of dissolved iron and other bioactive trace metals (Mn, Ni, Cu, Zn) in the Amundsen Sea Polynya, Antarctica. Elem: Sci Anthropocene, 3: 000071, doi:10.12952/journal.elementa.000071.

Sun J, Liu D Y, Ning X R, et al. 2003. Phytoplankton in Prydz Bay and its adjacent waters, Antarctica, during the summer of 2001/2002. Haiyang Yu Huzhao, 34 (5): 519-531, doi: 10.3321/j.issn:0029-814X.2003.05.

007 (in Chinese with English abstract).

Tortell P D, Long M C, Payne C D, et al. 2012. Spatial distribution of pCO_2, ΔO_2/Ar and dimethylsulfide (DMS) in polynya waters and the sea ice zone of the Amundsen Sea, Antarctica. Deep Sea Res Part II: Top Stud Oceanogr, 71-76: 77-93, doi:10.1016/j.dsr2.2012.03.010.

Turner J, Orr A, Gudmundsson G H, et al. 2017. Atmosphere-ocean-ice interactions in the Amundsen Sea Embayment, West Antarctica. Rev Geophys, 55(1): 235-276, doi:10.1002/2016RG000532.

Tynan C T. 1998. Ecological importance of the Southern Boundary of the Antarctic Circumpolar Current. Nature, 392(6677): 708-710, doi:10. 1038/33675.

Villafañe V E, Janknegt P J, Graaff M, et al. 2008. UVR-induced photoinhibition of summer marine phytoplankton communities from Patagonia. Mar Biol, 154(6): 1021-1029, doi:10.1007/s00227-008-0993-0.

Walker D P, Jenkins A, Assmann K M, et al. 2013. Oceanographic observations at the shelf break of the Amundsen Sea, Antarctica. J Geophys Res: Oceans, 118(6): 2906-2918, doi:10.1002/jgrc.20212.

Wallerstein P, Liebezeit G. 2009. Chapter 27: Determination of photosynthetic pigments//Grasshoff K, Kremling K, Ehrhardt M. Methods of seawater analysis, Third Edition. Weinheim; New York; Chiester; Brisbane; Singapore; Toronto: John Wiley & Sons, 557-566, doi:10.1002/9783527613984.ch27.

Wolf C, Frickenhaus S, Kilias E S, et al. 2013. Regional variability in eukaryotic protist communities in the Amundsen Sea. Antarct Sci, 25(6): 741-751, doi:10.1017/s0954102013000229.

Wright S W, Ishikawa A, Marchant H J, et al. 2009. Composition and significance of picophytoplankton in Antarctic waters. Polar Biol, 32(5): 797-808, doi:10.1007/s00300-009-0582-9.

Wright S W, van den Enden R L, Pearce I, et al. 2010. Phytoplankton community structure and stocks in the Southern Ocean (30–80°E) determined by CHEMTAX analysis of HPLC pigment signatures. Deep Sea Res Part II: Top Stud Oceanogr, 57(9-10): 758-778, doi:10.1016/j.dsr2.2009.06.015.

Zapata M, Rodríguez F, Garrido J L. 2000. Separation of chlorophylls and carotenoids from marine phytoplankton: a new HPLC method using a reversed phase C8 column and pyridine-containing mobile phases. Mar Ecol Prog Ser, 195: 29-45, doi:10.3354/meps195029.

Zhuang Y, Jin H, Li H, et al. 2014. Phytoplankton composition and its ecological effect in subsurface cold pool of the northern Bering Sea in summer as revealed by HPLC derived pigment signatures. Acta Oceanol Sin, 33(6): 103-111, doi: 10.1007/s13131-014-0495-5.